Plasmonics (2011) 6:35–42
DOI 10.1007/s11468-010-9166-3

Computational Study of Influence of Structuring of Plasmonic Nanolens on Superfocusing

Weixing Yu · Yongqi Fu · Lingli Li · Hongxin Zhang · Hua Liu · Zhenwu Lu · Qiang Sun

Received: 23 July 2010 / Accepted: 7 September 2010 / Published online: 15 September 2010

Abstract The focusing effect of the plasmonic nanolens is studied systematically. The influence of different construction parameters including the size of the central hole, the ring width of the surrounding concentric grating, the thickness of the metal film, and the distance of the central hole to grating has been simulated by rigorous finite difference time domain method and analyzed. It is found that the intensity of the central nano-spot is linearly proportional to the size of the central hole and inversely linearly proportional to the thickness of the metal film. In addition, the intensity of the lobes can be suppressed effectively by reducing the ring width down to a quarter of plasmon wavelength to achieve a better focusing effect. The influence of the distance of central hole to grating is a little bit complex, but generally, the intensity for the distance of $(2n-1)/2$ plasmon wavelength is larger than the case of the distance of $n\lambda_{SP}$. The simulation results can be a general guide for the design of plasmonic nanolenses.

Keywords Plasmonic nanolenses · Nanophotolithography · FDTD · Nanofocusing

W. Yu (✉)
State Key Laboratory of Applied Optics,
Changchun Institute of Optics, Fine Mechanics and Physics,
Chinese Academy of Sciences,
Changchun, Jilin 130033, China
e-mail: yuwx@ciomp.ac.cn

Y. Fu (✉)
School of Physical Electronics,
University of Electronic Science and Technology of China,
Chengdu 610054, Sichuan Province,
People's Republic of China
e-mail: yqfu@uestc.edu.cn

L. Li · H. Zhang · H. Liu · Z. Lu · Q. Sun
Opto-electronic Technology Center,
Changchun Institute of Optics, Fine Mechanics and Physics,
Chinese Academy of Sciences,
Changchun, Jilin 130033, China

L. Li
Chinese Academy of Sciences,
Beijing 10039, China

Introduction

Recently, plasmonic structure-based nanolithography becomes a hot research topic in areas of both optics and nanofabrication. Some interesting research works were reported such as plasmonic grating structures for contact photolithography [1], surface plasmon polariton-based interference lithography [2], dielectric/silver film-based nanolithography [3], and nanogap-assisted surface plasmon nanolithography [4]. Plasmonic structure contact photolithography technique has limited application because the structure is tightly in contact with photoresist during exposure. Interference lithography has limitations of the formation of one-dimensional or simple two-dimensional (2D) structures like square and cylindrical shapes. In contrast, plasmonic structure-based proximity photolithography is more attractive because a constant working distance or nanogap is kept during exposure. It means that the photoresist surface can be well kept and no damage occurs after exposure.

More recently, plasmonic lenses are appealing due to its subwavelength resolution for imaging and superfocusing. Many types of plasmonic lenses were reported such as width modulation-based lenses [5–9], elliptical nanopinhole lens [10], single circular ring-based lens [11–13], circular pinholes lens [14], nanowaveguide focusing [15], and radial

polarization-based circular grating lens [16, 17]. Plasmonic lenses-based photolithography has advantages of flexible formation or writing such as arbitrary 2D shapes and even 3D shaping by point-by-point writing technique. However, the lenses for the purpose of nanophotolithography need nanoscale lateral resolution and strong electric intensity. Considering this, we put forth a metallic periodic annuals structure which can act as a plasmonic nanolens for nanophotolithography use. Computational calculation and analyses were carried out on the basis of finite difference and time domain (FDTD) algorithm for the purpose of optimum design of the nanolens so as to obtain the lenses that possess nanoscale lateral resolution and strong E-field intensity. Our calculation results demonstrated that it is possible to realize the requirements in near-field region of around 20-nm working distance.

Structure Construction and Simulation Setup

Figure 1a shows the schematic diagram for the computational simulation. Figure 1b is top view of the plasmonic nanolens. The plasmonic nanolens consists of a central hole and a concentric ring grating which are all etched through into the silver film. The Ag film is coated on quartz substrate. Period of the grating is set as a plasmon wavelength λ_{SP} which for our case here is 490 nm for a linear polarization-based incident wavelength of 514 nm. The incident light is a linearly x-polarized plane wave with amplitude of 1 which propagates along the positive Z direction.

In our FDTD, three-dimensional (3D) calculations, simulation time and mesh size are 100 fs and $\Delta x=\Delta y=\Delta z=2$ nm, respectively. Drude model was employed modeling optical constants of the metal. The perfectly matched layer boundary condition was applied at the grid boundaries.

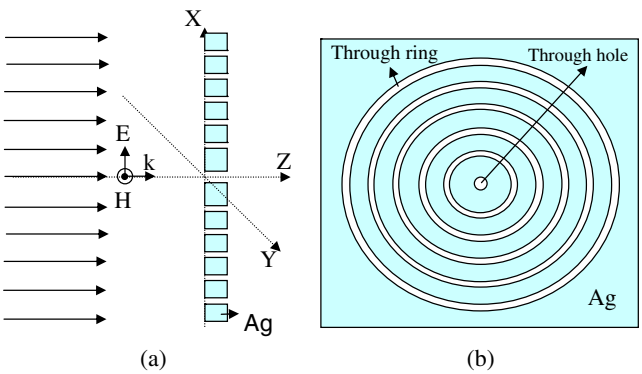

Fig. 1 Schematic diagram of the simulation setup (**a**) and the top view of the plasmonic nanolens (**b**)

Results and Discussions

Figure 2a shows the E-field distribution at $Z=20$ nm away from exit plane of the plasmonic lens on x–y plane. Here, the plasmonic lens has a structure described above with a central hole diameter of 70 nm and a distance of the inner concentric grating to the central hole of 1.04 μm. As can be seen, the surface plasmon wave is well focused and confined into the central hole. The amplitude of electric field $|E_x|$ is 2.54, which shows that the E-field is enhanced in comparison to the input field. The central-focused beam spot has an elliptical shape with size of 145 nm×87 nm at the site of full width at half-maximum E-field amplitude. Figure 2b shows the E-field distribution just after the plasmonic lens on x–z plane with $y=0$. As can be seen, the E-field intensity decays, and there is no focusing spot after the plasmonic lens (in free space). The E-field amplitude is the largest, with a value of 3.5 on back surface of the plasmonic lens, and it drops to 1 only after increasing the propagation distance to $Z=100$ nm. In fact, the E-field intensity decays along Z-axis as a function of e^{-z} as shown in Fig. 2c, which is the signature mark of the evanescent surface wave.

In comparison with the plasmonic microzone plate-like structures reported in [5, 6], the superfocusing property of the plasmonic nanolens considering in this work is significantly different. For plasmonic nanolens, the focusing point is located near the exit plane of the nanolens which means the focal length is near zero. On the other hand, for the plasmonic microzone plate, the focusing point is located outside free space of the lens and the focal length is at the wavelength scale.

In the section below, we will investigate and analyze the influence of the different structural parameters including the size of the central hole, the ring width, the distance of the central hole to grating, and the silver film thickness on the E-field distribution after the plasmonic lens from nanolenses structuring point of view.

Influence of Ring Width on E-field Distribution

Simulation parameters were set as follows: silver film thickness of 150 nm, and the diameter of the center hole of 100 nm. Figure 3 shows the E-field distribution at $Z=$ 20 nm away from the nanolens for different ring width along x-axis (see Fig. 3a) and y-axis (see Fig. 3b), respectively.

As can be seen, the shape of the central beam spot is elliptical which is due to the linear polarization of the incident beam. It can be formed to be circular by use of radial polarization beam [17]. It was reported that a special grating-like microstructure can be employed for the purpose of generation of radial polarization [18, 19]. The micro-

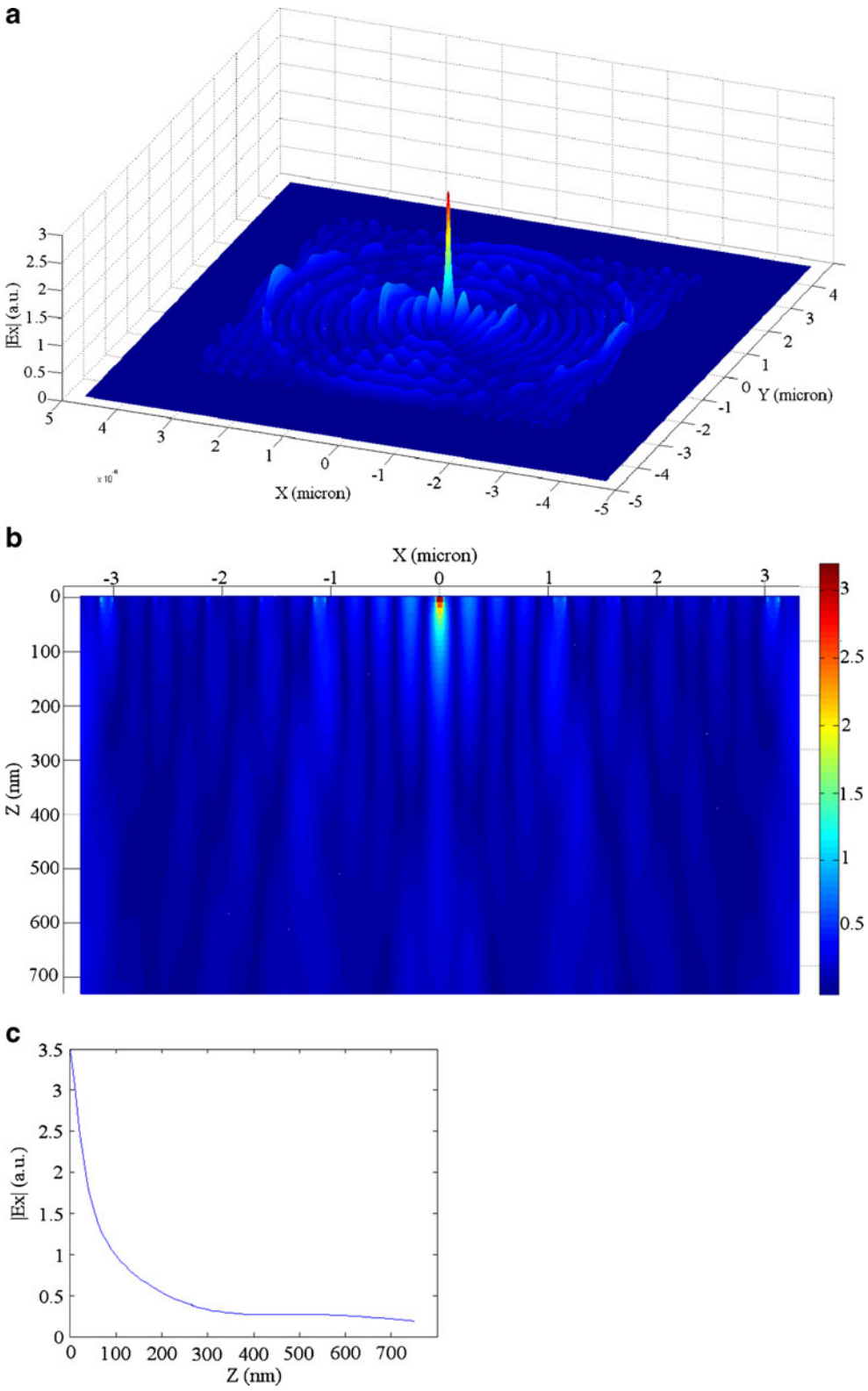

Fig. 2 **a** E-field distribution $|E_x|$ on x–y plane. **b** E-field distribution $|E_x|$ on x–z plane with $y=0$. **c** E-field distribution $|E_x|$ along Z-axis

structure is suitable to be integrated at backside of the nanolenses here for the formation of circular-focused beam spot. The E-field intensity strongly depends on the ring width. Generally, the larger the ring width, the higher the intensity of the center beam spot will be. For the side lobes, the intensity distribution along x-axis shows strong focusing effect and the amplitude is generally no larger than 1. However, the intensity distribution along y-axis strongly

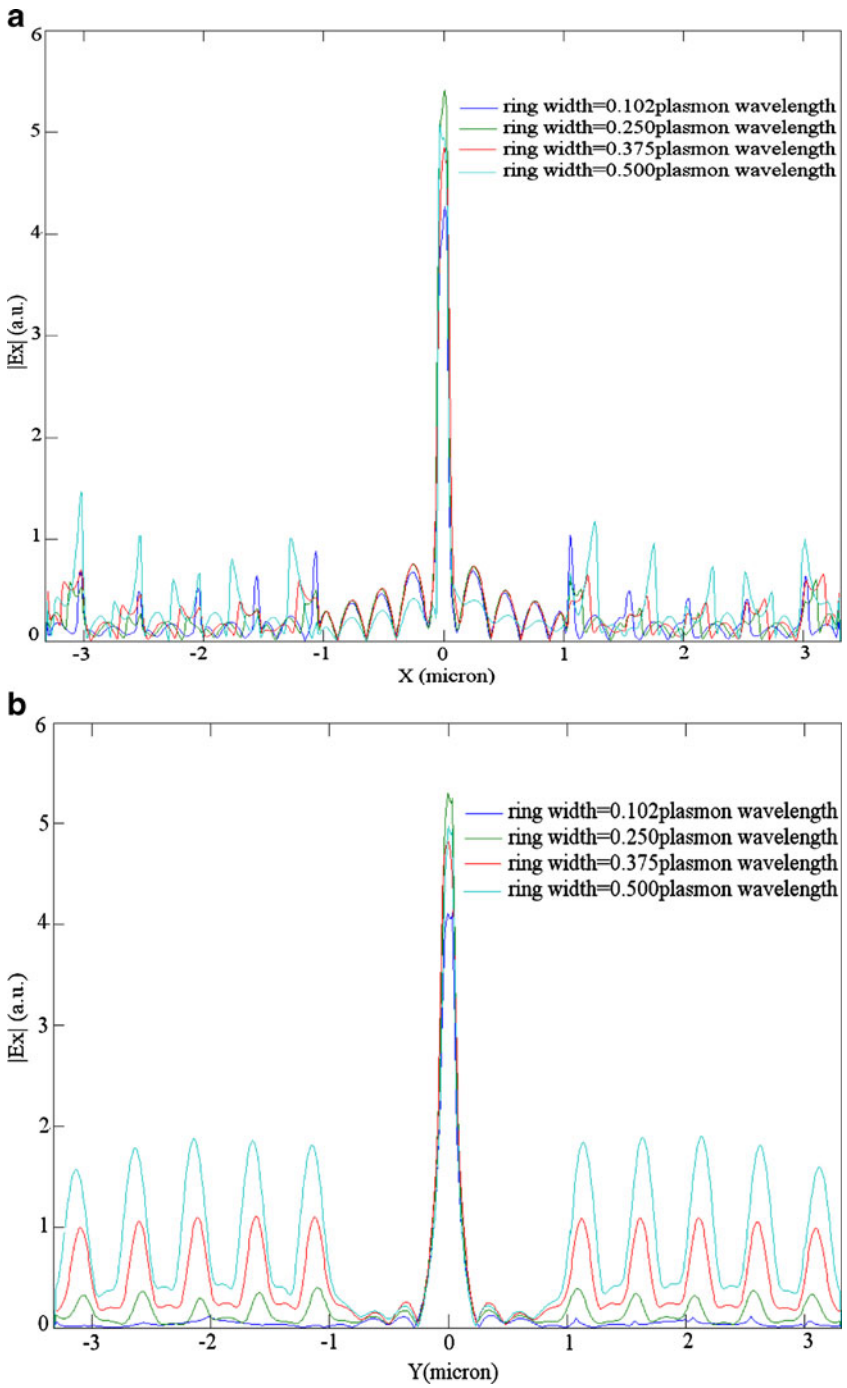

Fig. 3 E-field distribution for different ring width. **a** Electric-field distribution $|E_x|$ along x-axis. **b** Electric-field distribution $|E_x|$ along y-axis

depends on the ring width. As can be seen, the amplitude of E-field is nearly 2. Only when ring width is smaller than a $1/4\lambda_{SP}$, the amplitude of E-field along y-axis will be smaller than 0.5.

Influence of Size of Central Hole on E-field Distribution

Simulation parameters were set as follows: silver film thickness of 150 nm, and ring width of $0.102\lambda_{SP}$. Figure 4 shows the E-field distribution at Z=20 nm away from the nanolens for different central hole sizes along x-axis (see Fig. 4a) and y-axis (see Fig. 4b), respectively.

As can be seen, the shape of the central beam spot is elliptical in all cases. The E-field intensity for the central beam spot strongly depends on the size of the central hole. When the central hole diameter is 70 nm, the amplitude drops to almost half of the case when central hole diameter is 100 nm. When the central hole diameter is 50 nm, the amplitude drops to almost one-fifth of the case when central hole diameter is 100 nm. From nanofabrication point of

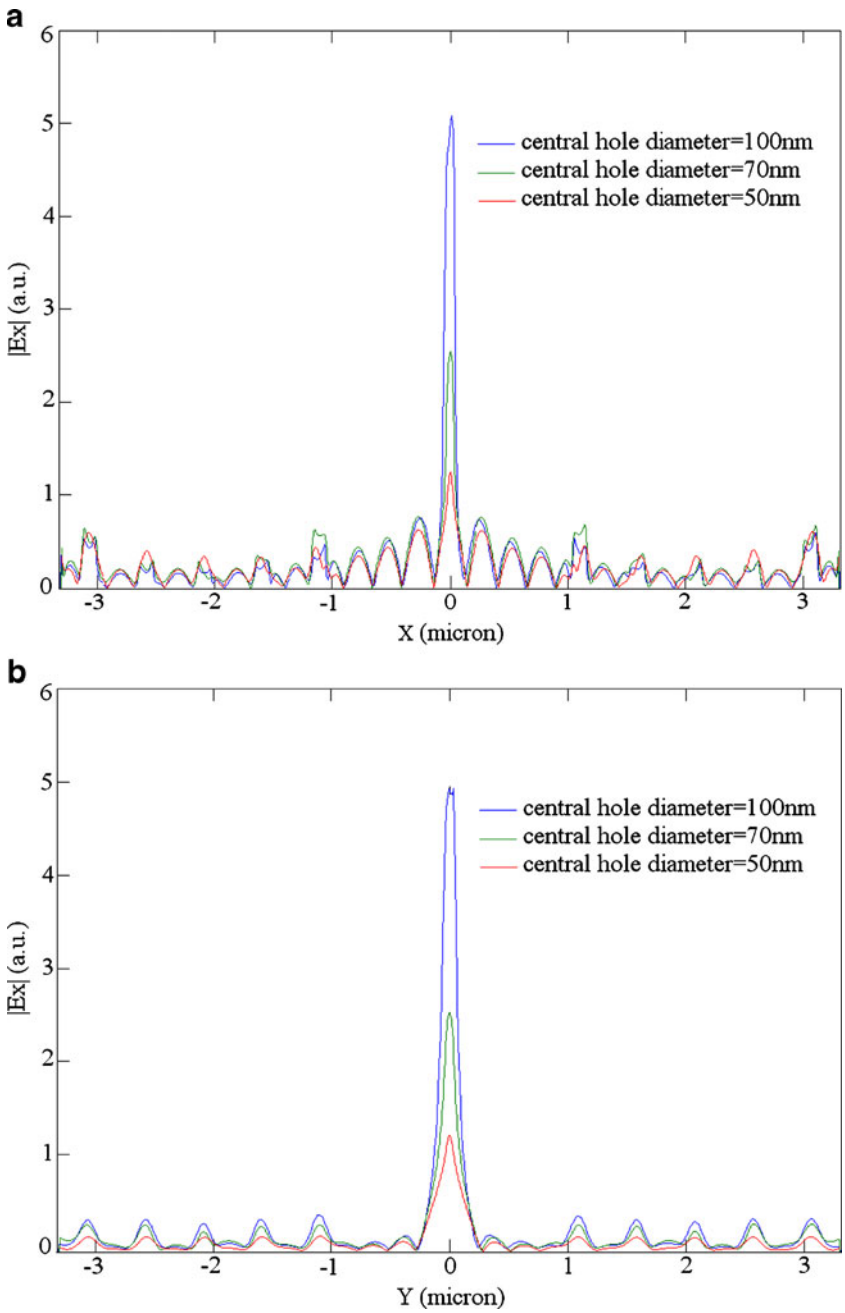

Fig. 4 E-field distribution for different central hole sizes. **a** Electric-field distribution $|E_x|$ along x-axis. **b** Electric-field distribution $|E_x|$ along y-axis

view, the central aperture will be V-shaped instead of the ideal case of vertical sidewall by means of the commonly used focused ion beam (FIB) technique [20]. The cone angle strongly depends on the thickness of metal film due to aspect ratio issue. As our previous calculation, the V-shaped aperture plays a positive role for the enhancement of the E-field.

Influence of Silver Film Thickness on E-field Distribution

Simulation parameters were set as follows: central hole diameter of 100 nm, and ring width of a quarter plasmon wavelength. Figure 5 shows the E-field distribution at Z= 20 nm away from the nanolens for different silver film thicknesses along x-axis (see Fig. 5a) and y-axis (see Fig. 5b), respectively.

As can be seen, the shape of the central beam spot is elliptical in all cases. The E-field intensity for the center beam spot strongly depends on the silver film thickness. Generally, the smaller the film thickness, the higher the intensity for the central beam spot will be. When silver film thickness is set to 75 nm, the corresponding amplitude of the E-field is around 8. When the silver film thickness is increased to 225 nm, the amplitude

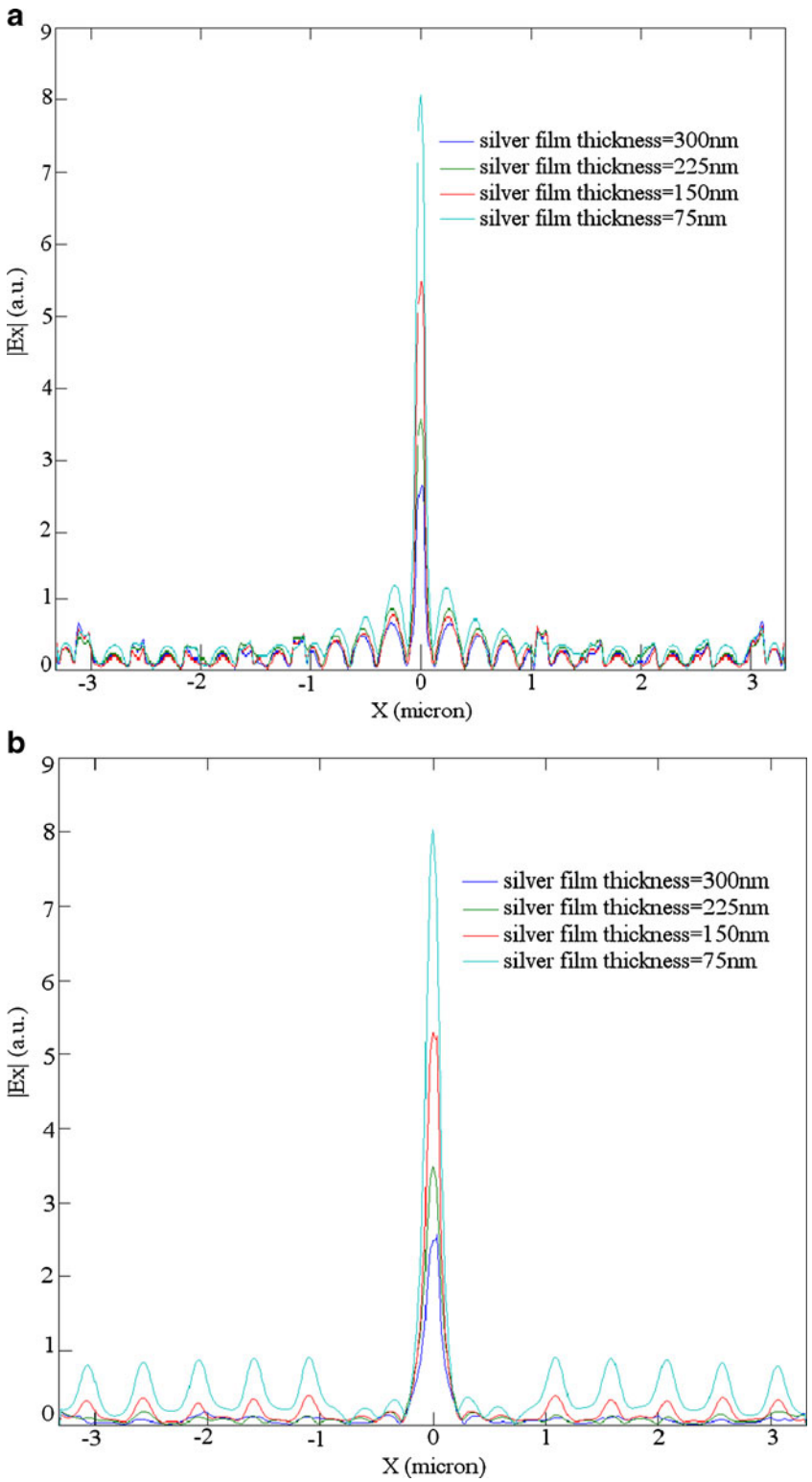

Fig. 5 E-field distribution for different silver film thickness. **a** Electric-field distribution $|E_x|$ along y-axis. **b** Electric-field distribution $|E_x|$ along y-axis

drops to less than 4. For intensity of side lobes, generally, the silver film thickness has ignorant effect for the E-field along x-axis. However, the intensity of side lobes along y-axis depends strongly on silver film thickness. As can be seen from Fig. 4b, the smaller the film thickness, the higher the intensity of the side lobes will be. When silver film thickness reaches 75 nm, the amplitude for side lobes is about 1. When silver film thickness is increased to be 150 nm, the amplitude of the side lobes quickly drops to less than 0.5.

In the case of the extreme case of the Ag thicknesses of 1–2 nm or less, on the one hand, theoretically, for the visible light incidence, when the Ag film thickness is less than its skin depth (~20 nm for Ag film), the incident light will totally transmit through the film, and no focusing can be formed accordingly. On the other hand, from nanofabrication point of view, it is too difficult to control the film coating and patterning process for the thickness of 1–2 nm or less. Therefore, we have not extended our calculation for the ultra-thin Ag film in this paper.

Influence of Distance of Rings to Central Hole on E-field Distribution

Simulation parameters were set as follows: central hole diameter of 100 nm, ring width of $1/4\lambda_{SP}$, and film thickness of 150 nm. Figure 6 shows the E-field distribution at Z=20 nm away from the exit plane for different distances of the rings to central hole along x-axis (see Fig. 6a) and y-axis (see Fig. 6b), respectively.

As can be seen, the shape of the center beam spot is elliptical in all cases. The E-field intensity for the center

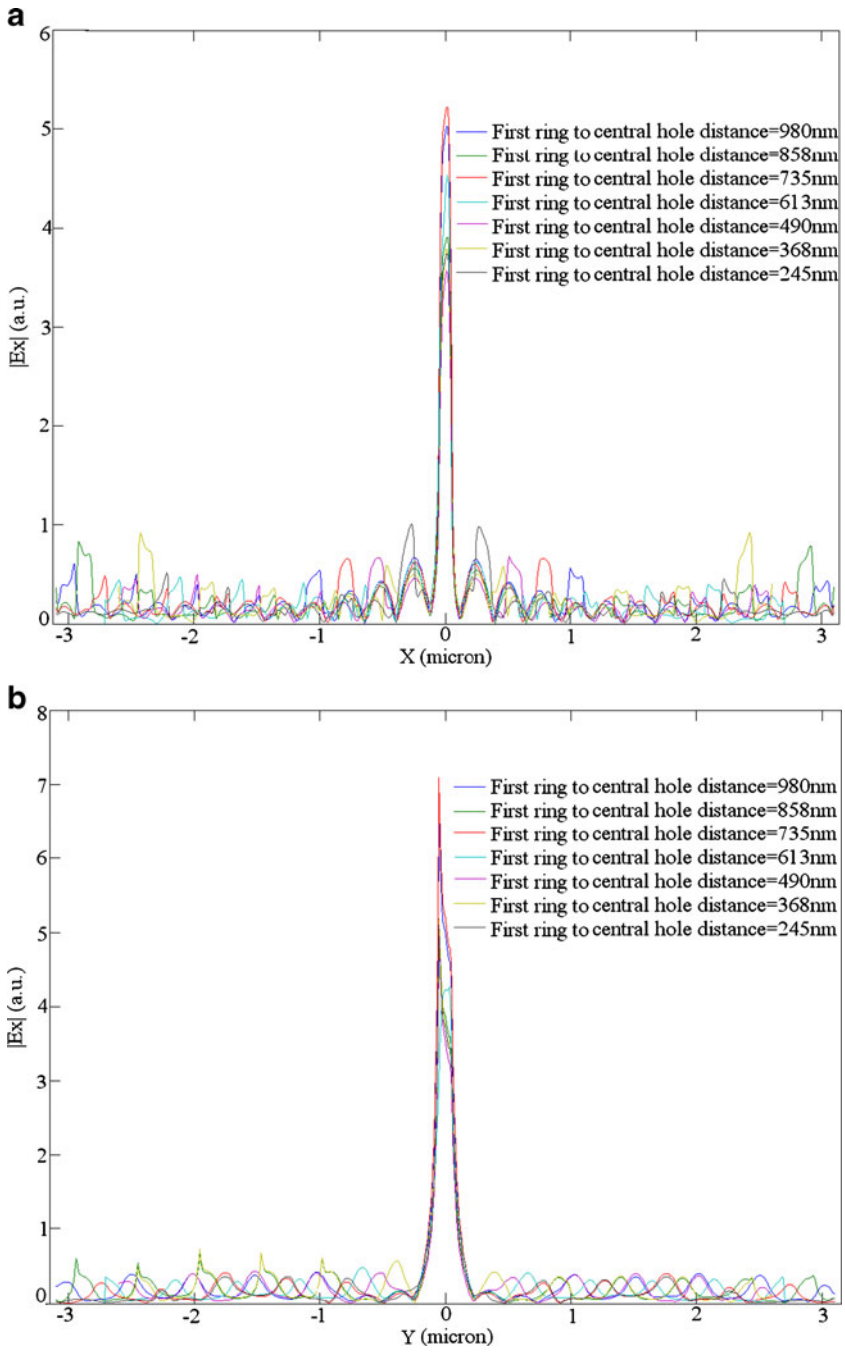

Fig. 6 E-field distribution for different distances of central hole to grating. **a** Electric-field distribution $|E_x|$ along x-axis. **b** Electric-field distribution $|E_x|$ along y-axis

beam spot strongly depends on the distance of grating to central hole. However, relationship between the intensity of the central beam spot does not linearly depend on the distance of grating to central hole. As can be seen, the highest intensity appears at the distance of 735 nm, which corresponds to $1.5\lambda_{SP}$. The lowest intensity appears at the distance of 490 nm, which corresponds to one plasmon wavelength. In general, the intensity for the distance of $(2n-1)/2\lambda_{SP}$, whereas n is an integer, is always larger than that of the distance of $n\lambda_{SP}$. The reason for this phenomenon can be simply attributed to the destructive or constructive interference of the surface plasmon waves at different propagation distances when they meet [11, 12].

In addition, for FIB nanofabrication issue, Ga^+ implantation will be unavoidable due to inherent characteristics of FIB process while directly etching the structure on Ag surface [21]. It causes increase of refractive index of Ag. Theoretically, the increased refractive index of metal film will make positive contribution on nanofocusing.

Summary

In summary, we have systematically studied the focusing effect of the plasmonic nanolens by employing the rigorous FDTD method. The influence of different construction parameters on focusing performance, including the size of the central hole, the ring width of the surrounding concentric grating, the thickness of the metal film, and the distance of the central hole to grating has been investigated. It is found that the intensity of the central nano-spot is linearly proportional to the size of the central hole, and inversely linearly proportional to the thickness of the metal film. In addition, intensity of the side lobes can be suppressed effectively by reducing the ring width down to a quarter of plasmon wavelength to achieve a better focusing effect. The influence of the distance of central hole to grating is a little bit complex. But, generally, the intensity at the distance of $(2n-1)/2\lambda_{SP}$ is larger than that of the case at the distance of $n\lambda_{SP}$. Although in our simulation, only silver film was investigated, we believe that the conclusion should be similar for other plasmonic metal materials such as Au and Al.

Acknowledgments The authors acknowledge the financial support from the National Natural Science Foundation of China with grant numbers 90923036 and 609770410. The work was supported by the National Natural Science Foundation of China (No. 60877021).

References

1. Luo X, Ishihara T (2004) Surface plasmon resonant interference nanolithography technique. Appl Phys Lett 84:4780–4782
2. X Jiao, P Wang, D Zhang, L Tang, H Ming, J Xie (2005) Nanolithography structure using surface plasmon interference with a planar silver lens. Progress in Electromagnetics Research Symposium, Hangzhou, China, 22–26 August 2005
3. Srituravanich W, Fang N, Sun C, Luo Q, Zhang X (2004) Plasmonic nanolithography. Nano Lett 4:1085–1088
4. Ueno K, Takabatake S, Nishijima Y, Mizeikis V, Yokota Y, Misawa H (2010) Nanogap-assisted surface plasmon nanolithography. J Phys Chem Lett 1:657–662
5. Fu Y, Zhou W, Lim LEN, Du CL, Luo XG (2007) Plasmonic microzone plate: superfocusing at visible regime. Appl Phys Lett 91:061124
6. Fu Y, Liu Y, Zhou X, Zhu S (2010) Experimental demonstration of focusing and lasing of plasmonic lens with chirped circular slits. Opt Express 18:3438–3443
7. Jia B, Shi H, Li J, Fu Y, Du C, Gu M (2009) Near-field visualization of focal depth modulation by step corrugated plasmonic slits. Appl Phys Lett 94:151912
8. Yuan HX, Xu BX, Lukiyanchuk B, Chong TC (2007) Principle and design approach of flat nanometallic surface plasmonic lens. Appl Phys A Mater Sci Process 89:397–401
9. Ko H, Kim HC, Cheng M (2008) Light transmission through a metallic/dielectric nano-optic lens. J Vac Sci Technol B 26:2188–2191
10. Fu Y, Zhou X, Liu Y (2010) Ultra-enhanced lasing effect of plasmonic lens structured with elliptical nano-pinholes distributed in variant period. Plasmonics 5:111–116
11. Liu Z, Steele JM, Srituravanich W, Pikus Y, Sun C, Zhang X (2005) Focusing surface plasmons with a plasmonic lens. Nano Lett 5:1726–1729
12. Liu Z, Steele JM, Lee H, Zhang X (2006) Tuning the focus of a plasmonic lens by the incident angle. Appl Phys Lett 88:171108
13. Steele JM, Liu Z, Wang Y, Zhang X (2006) Resonant and non-resonant generation and focusing of surface plasmons with circular gratings. Opt Express 14:5664–5670
14. Fu Y, Zhou W, Lennie LEN (2008) Nano-pinhole-based optical superlens, Research Letter in Physics, 148505
15. Xiuli Z, Fu Y, Shi-Yong W, An-Jing P, Zhong-Heng C (2008) Funnel-shaped arrays of metal nano-cylinders for nano-focusing. Chin Phys Lett 25:3296–3299
16. Lerman GM, Yanai A, Levy U (2009) Demonstration of nano-focusing by the use of plasmonic lens illuminated with radially polarized light. Nano Lett 9:2139–2143
17. Zhan Q (2009) Cylindrical vector beams: from mathematical concepts to applications. Adv Opt Photonics 1:1–57
18. Lerman GM, Levy U (2008) Generation of a radially polarized light beam using space-variant subwavelength gratings at 1064 nm. Opt Lett 33:2782–2784
19. Levy U, Tsai Chia-Ho, Pang L, Fainman Y (2004) Engineering space-variant inhomogeneous media for polarization control. Opt Lett 29:1718–1720
20. Fu Y, Zhou W, Lennie LEN, Du C, Shi H, Wang C, Luo X (2007) Influence of V-shaped plasmonic nanostructures on beam propagation. Appl Phys B 86:461–466
21. Fu Y, Bryan NKA (2005) Investigation of physical properties of quartz after focused ion beam bombardment. Appl Phys B 80:581–585